Ultra-Wideband Flat Metamaterial GRIN Lenses Assisted With Additive Manufacturing Technique

Shiyu Zhang, Ravi Kumar Arya, *Member, IEEE*, William G. Whittow, *Senior Member, IEEE*, Darren Cadman, Raj Mittra, *Life Fellow, IEEE*, and J. C. Vardaxoglou, *Fellow, IEEE*

***Abstract*— This article presents the designs of ultrawideband microwave flat gradient index (GRIN) lenses, which realizes over a 108% fractional bandwidth (12–40 GHz). The frequency-independent ray optics method is employed to determine the radially varying permittivity profile of the lenses. The challenge of realizing such a radially varying profile and the limitations in dielectric material choices are overcome by two additive-manufacturing-aided approaches: 1) partially infilled dielectrics with a varied periodicity, which ensures the lens performance at the higher end of the frequency range and 2) artificially engineered dielectrics (AED) with subwavelength-scale metallic inclusions, which enables-high permittivity dielectrics and leads to benefits of thickness and mass reduction for the GRIN lenses. Measured results demonstrate that the GRIN lenses improve the gain of open-ended waveguide sources by 8.7–15.6 dB over a wide frequency range from 12 to 40 GHz, with the realized gain of up to 23.6 dBi. Both the simulation and measurements of the presented design confirm the potential of implementing the proposed GRIN lens design in high directivity and beamforming antenna applications, across an ultrawideband frequency range.**

***Index Terms*— Additive manufacturing (AM), effective permittivity, flat grin lenses, metamaterials, millimeter waves, 3-D-printing, ultrawideband.**

I. Introduction

CONVEX lenses are well-known optical devices that converge impinging parallel rays to a spot at the focal point. Similarly, the lenses can be used as collimating devices that transform the wave from the focal point into a plane wave to realize a highly directive beam. Rather than having a conventional convex lens that is made from a homogenous material with a curvature of the surface profile, it is possible to fabricate these lenses with a flat profile to simplify their mounting. Such a design is commonly referred to as a gradient index (GRIN) lens [1], whose refractive index varies locally to manipulate the ray paths. The flat GRIN lenses have great potential for antenna applications in realizing high directivity [2]–[4] and beamsteering [5]–[7].

Compared with other flat lenses or beam-collimation devices, such as a Fresnel zone plate lens [8], [9], transmit array [10], [11], and superstrates [12], [13], whose designs are typically based on a specific target frequency and, thus, lead to a relatively narrow band, a GRIN lens can offer an extremely large bandwidth. The radially varied index profile can be designed based on transformation optics [14], [15] or ray optics [16] to ensure the broadband antenna gain improvement. However, practical demonstrations appearing in the literature only have shown up to 66% fractional bandwidth and only with an 8-dB gain improvement. Here, a GRIN lens design based on the ray optics method is presented, realizing broadband beam-collimation over a 108% fractional bandwidth, together with a gain improvement of 8.7–15.6 dB.

The GRIN lenses are generally designed with radially varying refractive indexes that are challenging to fabricate in practice. The most common approach to realizing a GRIN medium is to employ metamaterials realized by using stacked printed circuit boards (PCBs) [17]–[21], which is a complex process. Precise alignment and micromachining are involved for the multilayer stacked PCB structures, which prevents manufacturing on a large scale. Furthermore, some metamaterials with resonant-particle inclusions suffer from narrow bandwidth and losses. On the other hand, some authors have used additive manufacturing (AM) to realize GRIN lenses [22]–[24], which offers a cost-effective and repeatable approach. However, one of the challenges of widely deploying AM to fabricate RF components is the limited option of materials. Common AM materials, such as polymer-based thermoplastics, such as acrylonitrile butadiene styrene (ABS) and polylactic acid (PLA), and ultraviolet sintered resins, have relative permittivities (ε_r) that are on the order of 2.5∼3 and tan δ of 0.004∼0.03. The lack of choice of materials limits the popularity of AM in applications requiring a high refractive index.

This article presents a novel and low-cost solution to design and additively manufacture a flat GRIN lens, which offers ultrawideband performance and overcomes the limitation of material choices. To the best of our knowledge, the concept of

Manuscript received May 19, 2020; revised October 8, 2020; accepted November 24, 2020. Date of publication December 21, 2020; date of current version July 7, 2021. This work was supported in part by U.K. Engineering and Physical Sciences Research Council (EPSRC) Doctoral Prize Research Fellowship and in part by EPSRC Grand Challenge "Synthesizing 3D Metamaterials for RF, Microwave, and THz Applications" (SYMETA) under Grant EP/N010493/1. *(Corresponding author: Shiyu Zhang.)*

Shiyu Zhang, William G. Whittow, Darren Cadman, and J. C. Vardaxoglou are with the Wolfson School of Mechanical, Electrical and Manufacturing Engineering, Loughborough University, Loughborough LE11 3TU, U.K. (e-mail: s.zhang@lboro.ac.uk).

Ravi Kumar Arya is with the National Institute of Technology Delhi, New Delhi 110040, India.

Raj Mittra is with the Department of Electrical and Computer Engineering, University of Central Florida, Orlando, FL 32816-2993 USA, and also with the Department of Electrical and Computer Engineering, King Abdulaziz University, Jeddah 21589, Saudi Arabia.

Color versions of one or more figures in this article are available at https://doi.org/10.1109/TAP.2020.3044586.

Digital Object Identifier 10.1109/TAP.2020.3044586

utilizing the ray optics method to realize ultrawideband GRIN lenses for microwave applications has not been presented elsewhere heretofore. Frequency coverage in the range of 12–40 GHz is demonstrated in this work although the design can be scaled to realize lenses in a higher frequency range. Furthermore, this article details two approaches for tailoring the radially varied ε_r for the GRIN lenses. The first of these is to use the partially infilled dielectric that is realized by using the low-cost fused filament fabrication (FFF) technique. The AM process enables embedded subwavelength internal air voids in the 3-D object without requiring machining. Unlike perforating a solid material by removing parts from the raw materials, AM designs can be easily modified and rapidly prototyped with minimal material waste. The volume fraction of the internal air voids in the 3-D-printed geometries is used to tailor the effective permittivity (ε_{reff}) locally. The 3-D-printed unit cell with a varying periodicity has been utilized to ensure the broadband performance of the lens. The second approach, named the artificially engineered dielectric (AED), entails the addition of one double-sided PCB to the 3-D-printed dielectrics, which gives an extra degree of freedom in creating bespoke high-permittivity (ε_r) materials to realize GRIN lenses that are thin or have short focal lengths. The periodicity and the patch size are chosen to be nonresonant subwavelength scale, avoiding the issues of high loss, narrow bandwidth, and dispersion from the resonant-particles-based metamaterials and ensuring that the lenses would be ultrawideband. Furthermore, minimizing the number of PCB layers circumvents the need to align the PCB unit cells and reduces the overall cost in the process.

The designs of three lenses are presented and compared side-by-side in this article; these are: 1) thick lens fabricated by only using standard ABS materials; 2) thin lens with ∼30% thickness and ∼20% mass reduction by that utilizes the high-ε_r AED designs; and 3) thin lens fabricated by using high-ε_r FFF material, which mimics the AED lens and enables us to verify the performance of the AED materials. Besides the novel AED-based concept lens, the authors believe that the third lens is also a first-ever high-ε_r multimaterial device for RF applications, which has been 3-D-printed in its entirety.

This article is organized as follows. Section II details the design of GRIN lenses based on the ray optics approach. Section III shows the partially infilled dielectric unit cell with a varying periodicity that is fabricated using the FFF technique. Section IV introduces the AED approach, which increases the ε_r of an AM material to realize thickness reduction of the lens. Section V shows the performance characterization of all three lenses from 12 to 40 GHz. Section VI concludes this study.

II. GRIN Lens Design

The required variation in the refractive index can be calculated by equating the phase delay of the rays from the focal point until they exit the lens. It is sometimes assumed, for the sake of quick estimation [22], [25], that the ray paths inside the flat GRIN lens are straight lines, which disregards the relationship between the focal length and the lens thickness.

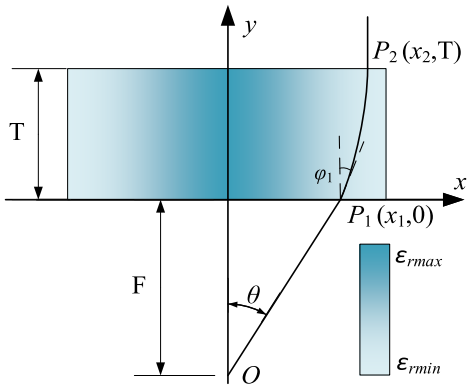

Fig. 1. Schematic of a GRIN lens with arc ray path inside the GRIN medium.

However, the true ray paths inside the GRIN medium are curved tracks, which leads to a greater phase delay than that of a straight ray path. Therefore, it is necessary to consider the arc length of the ray path for an accurate estimation of the phase.

The ray optics method for the arc ray path was first presented in [16] and applied to 3-D-printed lens design in [26]. However, the derivations of the method were not included in the literature. This section will show the mathematical representation of determining the inhomogeneous permittivity profile to convert the radiation between a spot and a plane wave.

The cross section of a flat GRIN lens, whose axis of symmetry is the focal axis shown in Fig. 1, has its maximum relative permittivity (or refractive index) at the center, and this index gradually decreases along the radius. The purpose of having such a GRIN is to ensure that all the rays that pass through the lens have equal phase at the exit plane $y = T$.

The ray path integral, which is based on Fermat's principle and satisfies the condition of equal phase delay of the rays from the focal point to where they exit the lens, is given by

$$F + n_{max}T = OP_1 + \int_{P_1}^{P_2} nds \tag{1}$$

where n_{max} is the refractive index at the center.

The arc ray path length inside the GRIN medium is determined as follows:

$$\int_{P_1}^{P_2} nds = \frac{T\left(3\varepsilon_{r1} - 2\sin^2\theta\right)}{3\sqrt{\varepsilon_{r1} - \sin^2\theta}}. \tag{2}$$

The derivations of (2) are given in the Appendix. Combining (1) and (2), we obtain a frequency-independent design equation for determining the variation of the permittivity ε_r at any location on the flat GRIN lens

$$\frac{T\left(3\varepsilon_r - 2\sin^2\theta\right)}{3\sqrt{\varepsilon_r - \sin^2\theta}} = T\sqrt{\varepsilon}_{rmax} + F - \frac{F}{\cos\theta}. \tag{3}$$

For a practical approach, it is necessary to know the maximum value of θ_{max}, which is determined by the diameter of the lens and its focal length. These parameters are usually predetermined based on the desired volume of the antenna system and the nature of the feed. Furthermore, it is equally

important to have knowledge of the minimum and maximum permittivities of the available materials. After determining the values of θ_{max} and ε_{rmin}, (3) can be used to find the lens thickness T. Generally, a small F and a lowε_{rmax} both result in a thick lens. The ε_r variation can be calculated for a series of given θ-values to produce an ε_r profile with respect to the locations at the lens. In practice, we can approximate the ideal smooth profile of ε_r with a stepped function and divide the lens into a series of concentric zones each with a different relative permittivity.

In this work, all the lenses were designed to have six dielectric rings; the ring widths were set to 10 mm. The lens thickness and the permittivity profile were determined by the available 3-D-printing materials.

III. 3-D-Printed Dielectric Unit Cell With Varied Periodicity

The entire lens can be fabricated by using the FFF with a single material and in a single process, without machining and assembling, by taking advantage of the AM process. The dielectric rings are printed by using a nonsolid internal structure with air voids, whose volumes can be used to adjust ε_{reff} of the medium [26]. Here, we use the material volume percentage (υ), which is determined by the ratio of the volume of the 3-D-printing material in the nonsolid printed structure, to the volume of the entire structure. The required volume percentage υ for tailoring the effective permittivity ε_{reff} of the 3-D-printed dielectrics can be approximately determined by

$$\upsilon = \frac{\varepsilon_{reff} - 1}{\varepsilon_{ro} - 1} \tag{4}$$

where ε_{ro} is the relative permittivity of the 100% 3-D-printing material.

The AM process typically slices the 3-D-geometry into a series of thin layers and fills them with periodic 2-D infill patterns. For ease of fabrication, the flat GRIN lens was 3-D-printed with the largest cross-sectional area sitting on the printing platform, which resulted in the periodical infill patterns in a plane with thin, sliced, circular layers. Fig. 2(a) shows the unit cell of the 3-D-printed infill pattern of the grid. The infill linewidth w, which is determined by the FFF machine extrusion nozzle diameter, is a constant parameter, and it is the minimum manufacturable feature size. The different material volume percentage υ was realized by the variable parameter d. Unlike conventional metamaterial unit cell designs that have a fixed periodicity, this unit cell has a variable period d because, in order to achieve a very low permittivity value, the unit cell must be large due to the restriction in the minimum manufacturable feature size (i.e., infill linewidth). However, the increased unit cell size would result in a reduced maximum operating frequency when the unit cell size approaches the wavelength. Thus, if a fixed periodicity of the unit cell is used for the entire lens, the upper end of the operating frequency of the lens is primarily determined by the largest unit cells. According to (3), a GRIN lens only requires low permittivity values (i.e., a large unit cell) in the outermost region of the lens; therefore, the inner part of the lens can have a small unit cell to ensure the inner region still functions at high frequencies. Hence, our unit cell design utilizes the variable unit cell size to allow a variable upper end of the operation frequency, which depends on the periodicity of the unit cell. This design method enables us to gradually increase its size from the center to the outer region of the lens, which extends the maximum operation frequency compared with lenses based on the unit cells with fixed periodicity.

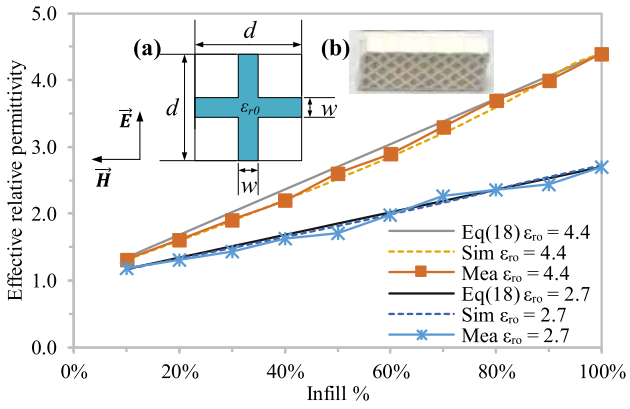

Fig. 2. Retrieved ε_{reff} as a function of material infill volume percentage for ABS ($\varepsilon_{ro} = 2.7$) and PREMIX ($\varepsilon_{ro} = 4.4$). (a) Unit cell of the 3-D-printed infill pattern. (b) Photograph of the 3-D-printed sample for NRW measurement.

In this work, we employed the FFF machine (Makerbot 2X) equipped with a 0.4 mm extrusion nozzle. The extruded linewidth was set to $w = 0.48$ mm since the linewidth expanded by approximately 20% due to heat expansion and extrusion pressure. The simulated ε_{reff} of this unit cell as a function of material volume percentage (realized by varying parameter d) for different ε_{ro}'s (different 3-D-printing filaments) is shown in Fig. 2. The simulation was carried out by using the periodic boundary condition in the CST Microwave Studio. $\varepsilon_{ro} = 2.7$ and $\varepsilon_{ro} = 4.4$ represented a normal ABS material ($\varepsilon_r = 2.7$ and $\tan\delta = 0.01$) and a high-ε_r 3-D-printing filament PREMIX PREPERM TP20280 ($\varepsilon_r = 4.4$ and $\tan\delta = 0.004$), respectively. The dielectric properties were also verified by the measured ε_{reff} at 10 GHz using an X-band waveguide and the Nicolson–Ross and Weir (NRW) method [27]. The photograph in Fig. 2(b) shows a 3-D-printed sample with the grid infill for the NRW measurement. Fig. 2 shows a close agreement between the simulated and measured results, and they all match those predicted by (18).

The polarization of the incident wave was also rotated from 0° to 45° in the plane with the unit cell, and the simulated ε_{reff} with different incident polarizations did not change. Since the fields illumined by the source were always parallel to the flat lens plane, this unit cell had an isotropic ε_{reff} in the unit cell plane, and the 3-D-printed lens was insensitive to the impinged fields' polarization. Thus, the lens can be mounted without perfectly aligning the unit cell with the emitted fields, which offers flexibility and practicability, and also the potential application for different polarization illuminations.

The lens performance depends on the number of dielectric rings and the maximum unit cell size. It is recommended

that the number of rings should be large enough to realize a smooth permittivity variation profile that reduces the aberrations. The ring width should be smaller than the wavelength at the maximum operating frequency to achieve the wideband performance. However, this results in very thin ring widths. If nonresonant metamaterials are used, the ring width should be greater than two unit cells to form an effective dielectric medium. This constraint is typically most relevant to the outermost ring as the outermost ring has the lowest permittivity and requires the largest unit cell. Therefore, the minimum ring width and ε_{reff} of the dielectric ring are based on FFF extrusion limitation on the value of parameter w and the choice of 3-D-printing material ε_{ro}. In this work, the lowest permittivity for the lens was set to $\varepsilon_{reff} = 1.24$ (realized by ABS, $\varepsilon_{ro} = 2.7$), and the ring width was 10 mm. A finer extrusion width w or smaller value of ε_{ro} both achieve lower ε_{reff} and allow a smaller unit cell size d, which leads to a thinner ring width with a smoother index variation in the lens. Furthermore, since the unit cell sizes at the lens center are small, the smoothness of the index variation could also potentially benefit from a radially varying ring width, which has finer ring widths toward the lens center and larger ring widths toward the edge. In this work, the 10 mm constant ring width provides a good balance between design complexity and lens performance in the frequency range of 12–40 GHz.

IV. AED Materials

Although new high index 3-D-printing materials (e.g., PREMIX PREPERM) offers an extra degree of freedom of AM material choice, the range of the fabricated index is still limited by the permittivity of the filament. The AEDs method enables tweaking ε_r of dielectric materials by using discrete square (other shapes can be used as well) metallic patches and print them on top (or bottom, or both on top and bottom) of the dielectric sheet to increase the desired ε_r values and, therefore, leads to a thin lens or a short focal length to facilitate compact and low-profile antennas. Alternatively, the metallic elements can be etched from a commercially available PCB laminate, and then, the etched laminate sheet is placed above another dielectric [see Fig. 3(a)].

This type of composite structure aims to provide ε_{reff} that is equivalent to the given ε_r from a standard equivalent dielectric [EQD, see Fig. 3(b)] material. This equivalence is evaluated using the transmission phase behavior, namely, the phase of S21 of the AED should be matched to that of the EQD. The property of the AED is tuned by the parameter patch length l. The l value should be smaller than the periodicity p and preferably be small to stay below resonance, so it ensures a broadband performance. However, due to the small cross-sectional area of the patches (see Fig. 3(a), front view), the cross-sectional area is determined by patch length l and the PCB metallization thickness (0.035 mm in this case); a single-layered patch has a limitation on maximum achievable ε_r. Therefore, having the patches etched on both sides and tuning the dimensions of the double-layered patches offer an extra degree of freedom in tailoring the permittivity over a wide range. The effective dielectric properties of the AED

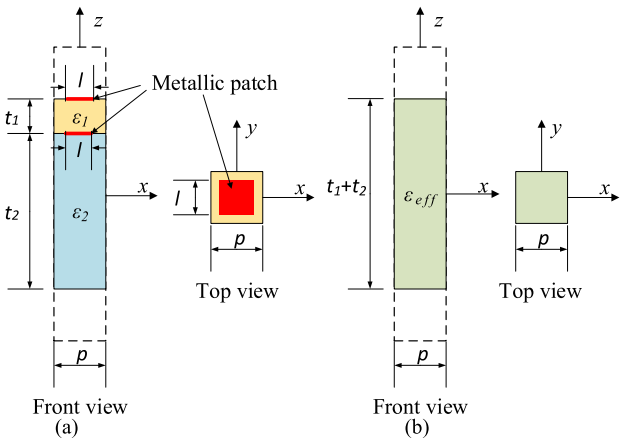

Fig. 3. Unit cell design of (a) AED with the stacked-patches-dielectrics structure and (b) EQD that provides the effective permittivity equivalent to the AED.

were investigated by using the periodical boundary condition in the CST Microwave Studio, with the periodicity p. It was found that the unit cell with periodicity smaller than $\lambda/5$ provided satisfactory results while avoiding the issues of high loss, narrow bandwidth, and dispersion, typically associated with metamaterials. The $< \lambda/5$ periodicity condition also ensured that the patch size was small enough to keep it below its resonance, which was the key to realizing a wideband design.

An AED lens was designed to have the same focal length (150 mm) and diameter (120 mm) as the 3-D-printed GRIN lens in [26] but aimed to reduce the overall thickness by ~30%. This required increasing ε_r of the center rings. The lens was designed to have six dielectric rings, and according to (17), the required ε_r values for the three inner rings are 2.90, 3.25, and 3.46, respectively. The values are all higher than the relative permittivity of conventional thermoplastic FFF materials, e.g., PLA and ABS, whose ε_r =~2.7. Although the required ε_r could be realized by using the high-ε_r FFF filament, here, we aimed to demonstrate the benefit of utilizing the AED approach in a scenario—there were no commercial-off-the-shelf specialized high-ε_r FFF materials available. For comparison, the high-ε_r FFF filament (PREMIX PREPERM) was used to fabricate the dielectrics with the same permittivities to evaluate ε_{reff} of AEDs.

Rogers RO4350B, with ε_r of 3.48 and $\tan\delta$ of 0.0037 at 10 GHz, was used as the top PCB. The design parameters of the unit cell were $t_1 = 1.52$ mm, $t_2 = 11.56$ mm, $p = 2$ mm, $\varepsilon_{r1} = 3.48$ (RO4350B), $\varepsilon_{r2} = 2.70$ (ABS), and the patch size, l, was variable depending on the desired permittivity value. CST Microwave Studio was used for simulating the AED and EQD unit cells. Floquet port excitations were set up in the positive and negative z-directions. The patches were arranged in a circular/Cartesian pattern, as shown in Fig. 4, which also shows its cross section. The dimensions of the patches were chosen to ensure the S21 phases of the AED structures matched those of the EQDs that have the desired ε_r values.

The simulated S21 of three AED unit cells are shown in Fig. 5 compared with the S21 of three EQD unit cells.

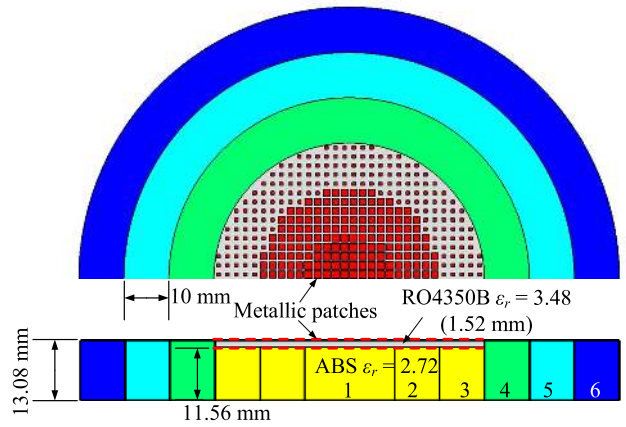

Fig. 4. Flat GRIN lens with metallic patches at the innermost three rings and cross section of the proposed GRIN lens enabled by AED.

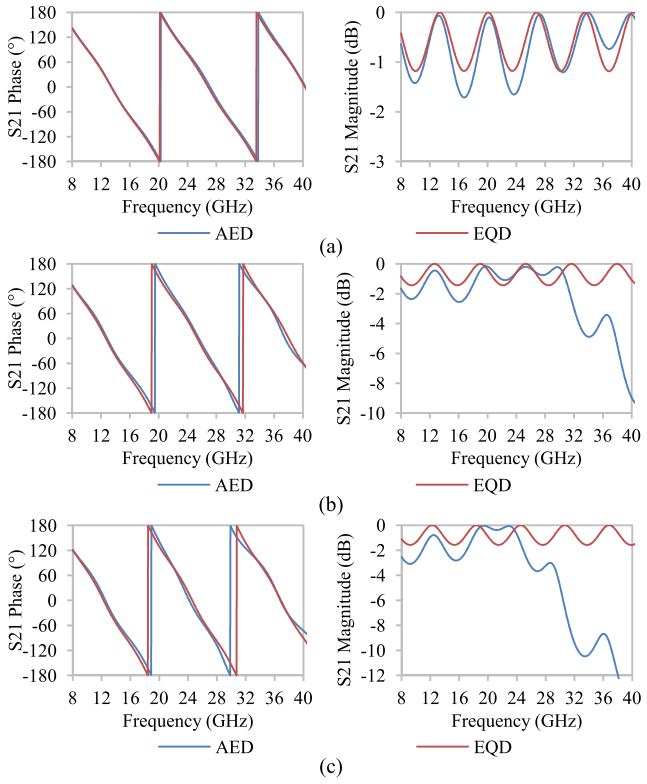

Fig. 5. Simulated S21 phase and magnitude of three AED unit cells that are equivalent to the homogeneous dielectric EQDs with ε_r of (a) 2.90, (b) 3.25, and (c) 3.46, respectively.

A close match of the S21 phases between the AEDs and EQDs was observed, which indicated that the AED could realize the same phase delays as those achieved by standard dielectrics. It is worth noting that, although the AED shows higher insertion loss compared with the EQDs, particularly when the patch size is close to the unit cell size (see Fig. 5(c) when $l =$ 1.72 mm), the lens performance does not exactly correlate with the S21 magnitude of the unit cell. This is because the unit cell simulation is based on the infinite periodical condition, but, in practice, the unit cells are only placed in a small region of the lens, and they have gradually changed geometries in order

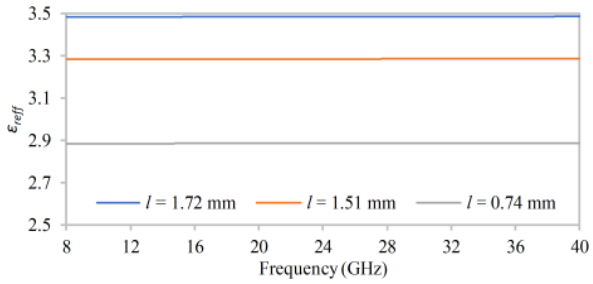

Fig. 6. Retrieved ε_{reff} permittivity over frequency of the proposed unit cell with different patch lengths.

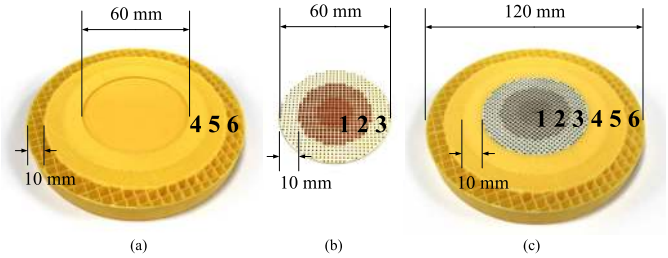

Fig. 7. Photographs of (a) 3-D-printed GRIN lens with a slot for AEDs, (b) GRIN AEDs that are made from RO4305B, and (c) assembled AED lens.

TABLE I
3-D-PRINTED LENS WITH AEDS

Ring NO.	ε_r	l (mm)	ABS v	d (mm)
1	3.46	1.72	100%	0
2	3.25	1.51	100%	0
3	2.90	0.74	100%	0
4	2.41	N/A	82.0%	0.83
5	1.84	N/A	48.8%	1.69
6	1.24	N/A	14.0%	6.61

to achieve the graded-index property. The measurement results of the AED lens will be presented in Section V.

Fig. 6 shows the ε_{reff} values of the AEDs that were retrieved by using the analytical method described in [28]. It is worthwhile to note that retrieving the ε_{reff} values is not essential for using the AED approach. This is because the AEDs and their EQDs can be considered as equivalent to each other in a lens, to provide equal phase delays, as long as their transmission phases are matched.

The radially varying ε_r values for the AED lens were calculated by using (17), and the required patch sizes of the AEDs are shown in Table I. ABS was used for printing the rest of the lens by employing the method described in Section III. The ABS infill factors for the three outer rings are shown in Table I. Note that the dielectric bases in the three inner rings of the lens were 3-D-printed with 100% ABS infill, and thus, there are no dielectric unit cells in these three rings (i.e., $d = 0$ mm). The fabricated lens is shown in Fig. 7.

In order to evaluate whether the AEDs can be truly used as the replacements of their EQDs for lens applications, a pure dielectric lens (named the EQD lens), which had the same thickness and permittivity profile as those of the AED lens,

TABLE II
PARAMETERS OF THE 3-D-PRINTED EQD LENS THAT WAS EQUIVALENT TO THE AED LENS

Ring No.	ε_r	ABS v	PREMIX v	d (mm)
1	3.46	N/A	72.4%	1.01
2	3.25	N/A	66.2%	1.15
3	2.90	N/A	55.9%	1.43
4	2.41	82.0%	N/A	0.83
5	1.84	48.8%	N/A	1.69
6	1.24	14.0%	N/A	6.61

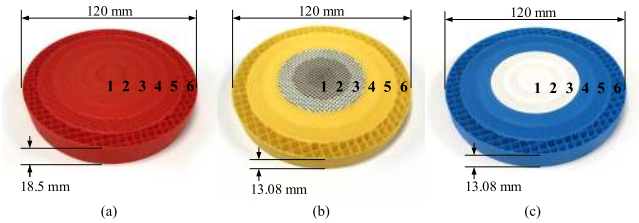

Fig. 8. Photographs of three flat GRIN lenses: (a) thick lens that is reproduced from [26], (b) AED lens, and (c) fully 3-D-printed EQD lens that is equivalent to the AED lens.

was fabricated for comparison. The three inner rings of this lens were made by using the EQDs that are equivalent to the three inner rings of the AED lens. PREMIX PREPERM TP20280 ($\varepsilon_r = 4.4$) was used for fabricating the three inner rings since the required ε_r could not be achieved by ABS. The ABS was used for the three outer rings. The reason for using normal ABS instead of the PREMIX material to fabricate the three outer rings was to ensure the EQD lens having the same outer three rings (in both material composition and infill volume percentage) as those of the AED lens.

The entire EQD lens was 3-D-printed in one single process by using a dual-extruder FFF printer (Makerbot 2X). The PREMIX material showed good compatibility and solid interface adhesion to the normal 3-D-printing ABS material. The radial variations of the ε_r of the EQD lens were the same as those of the AED lens, and the volume fraction of the ABS and PREMIX material is shown in Table II.

The lens reported in [26] was also reproduced to compare with the AED and EQD lenses. Fig. 8 shows the photographs of the three prototyped lenses. The lens in Fig. 8(b) is the AED lens that has the same focal length as the lens (a) (reproduced from [26]) but with a 5.42-mm-thick reduction. The lens in Fig. 8(c) is the EQD lens that had white PREMIX material for the three inner rings and blue ABS for the three outer rings. All three lenses were designed to deliver the same collimating performance to improve the gain of the source located at their focal points. For ease of identification, three lenses were printed with different colors. Dielectric measurements showed that there were no significant differences in ε_r ($\sim$2.7) and tan δ ($\sim$0.01) in the three lenses with different colors, which represented different fabrication samples based on an identical design.

V. RESULTS

The wideband performance of the designed lens was evaluated in the frequency range of 12–40 GHz. Ideally, the wideband GRIN lenses would need a wideband feed antenna. An ideal wideband feed antenna should have a consistent radiation pattern across the frequency band, a symmetric radiation pattern in E- and H-planes, and a stable phase center position [29]–[31]. In this work, three open-ended waveguides (OEWGs) were used as the feeds to cover the frequency bands Ku (12–18 GHz), K (18–26 GHz), and Ka (26–40 GHz), respectively, due to their relatively stable radiation patterns (the 3 dB beamwidth variation $< 7°$), and the gain (6–8 dBi) was similar in the different frequency bands. CST Microwave Studio simulations were carried out to investigate the near-field electric field and the far-field radiation patterns of the lenses. For simplicity, the waveguide port excitation was used instead of the coaxial to waveguide transition for exciting the OWEG feed. Although the partial in-filled structure had been proven earlier (see Fig. 2) to have an effective permittivity and behave as though it were comprised of a homogenous dielectric material, it was simulated under periodic boundary conditions (i.e., infinite number of unit cells). When the frequency approached 40 GHz, the 3-D printed largest unit cells in the outermost ring became potentially problematic since there were less than two unit cells in one ring width. Thus, the outer ring no longer provided the desired effective permittivity values. The unit cell size was less critical for the five inner rings since they were far smaller than the wavelength. In the simulations, the actual printed structure of the outermost ring of the lenses was modeled, and the five inner dielectric rings were simulated by using homogeneous effective properties to reduce the computational complexity. The permittivity and the loss tangent of the ABS and PREMIX materials were measured by using a split-post dielectric resonator at 2.4 GHz and the NRW method in the 8–12-GHz range. The measured dielectric properties were similar at 2.4 and 10 GHz. The relative permittivity of ABS materials and the PREMIX materials were 2.72 and 4.4, respectively, and the loss tangents of the ABS and PREMIX materials were 0.010 and 0.004, respectively. The measured dielectric properties were used in the simulation. The loss tangents of the homogeneous dielectrics ABS and the PREMIX were set to 0.010 and 0.004, respectively, regardless of the infill percentages. Consequently, the simulation results represent the worst case scenarios since, in reality, the loss tangent is reduced as we reduce the percentages of the in-fill.

The setups for measuring the radiation patterns are shown in Fig. 9. Fig. 10 shows the measured radiation patterns of the antenna at 15, 22, and 33 GHz and compares them with the simulated patterns. Close agreement was observed between the far-field patterns and the directional beams at $\theta = 0°$ among all three lenses, across the measured frequency range, and the sidelobe levels were all below -10 dB with respect to the main lobe.

As expected, it was found that the radiation patterns narrowed as the frequency was increased. The measured half-power beamwidths (HPBWs) across the frequency are shown in Fig. 11, both for the E- and H-planes. All three

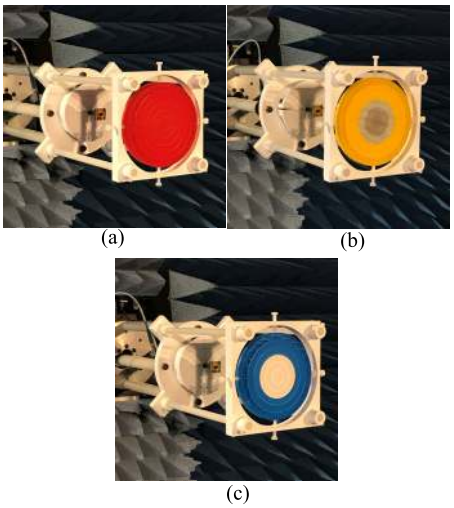

Fig. 9. Measurement setup with the 3-D-printed lenses with OEWG feed at the focal point of the lenses: (a) thick lens, (b) AED lens, and (c) EQD lens.

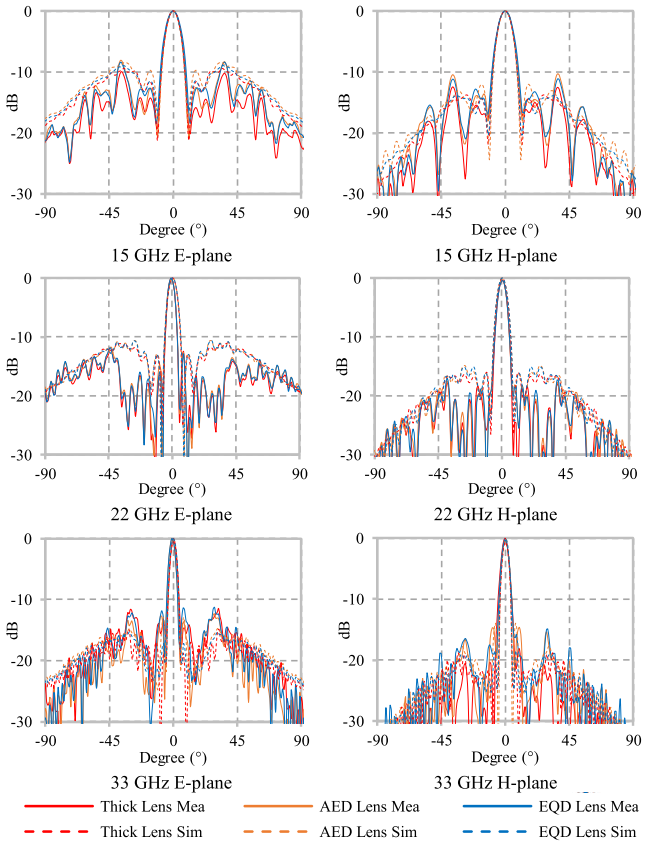

Fig. 10. Measured radiation patterns of the three lenses at 15, 22, and 33 GHz, respectively, compared with the simulated results.

lenses had similar HPBW levels in the E-plane, which started at ∼11° at 12 GHz and reduced to ∼3.6° as the frequency was increased to 40 GHz. The measured HPBW in the H-plane was slightly larger (by ∼0.7°) compared with that in the E-plane. This result clearly confirms that all three lenses worked equally well and generated pencil beams and facilitated highly directional antennas.

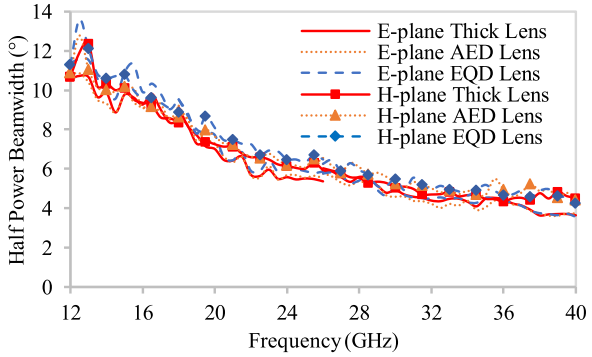

Fig. 11. Measured HPBW in the E- and H-planes in three frequency bands: 12–18, 18–26, and 26–40 GHz.

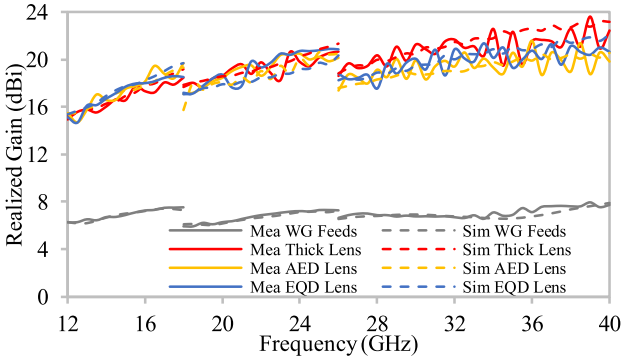

Fig. 12. Measured realized gain of three different lenses fed by OEWGs in three frequency bands: 12–18, 18–26, and 26–40 GHz compared with the simulated results.

The measured realized gain of the three OEWG-fed lenses is shown in Fig. 12 compared with simulations. All three lenses offered good wideband performance. The measured gain improvements from the three lenses show good agreement between each other, and this, in turn, serves to confirm the viability of using the AED approach to realize low-profile lenses in a low-cost and convenient manner. The root-mean-square (rms) differences between the measured and simulated gain over the frequency between 12 and 40 GHz of the thick lens, AED lens, and the EQD lens were 0.91, 0.85, and 0.93 dB, respectively. Meanwhile, the close match between the performance of the AED lens and the EQD lens demonstrates the possibility of using the AEDs to augment the properties of the dielectric materials and offer an extra degree of freedom in material selection. Both AED and EQD lenses had similar measured realized gains ranging from 15.1 dBi at 12 GHz to 23.6 dBi at 40 GHz, which implies that the gain of the feeds was enhanced by approximately 8.7–15.6 dB. The measured total antenna efficiency (efficiency = realized gain/directivity, including the mismatch) of the thick lens, AED lens, and the EQD lens had values of 82%, 83%, and 82%, respectively, when averaged over the frequency band from 12 to 40 GHz. All lenses had little effect on the S11 of the OEWG feeds, and all the OEWG feeds were well-matched; thus, the loss is mainly due to the dielectric loss. Simulations were carried out by using loss-less dielectrics, and the realized gain was improved up to 1.5 dB compared with the lossy dielectrics.

The results indicate that the gain of the thick lens is ∼2 dB higher than the AED lens at the higher end of the

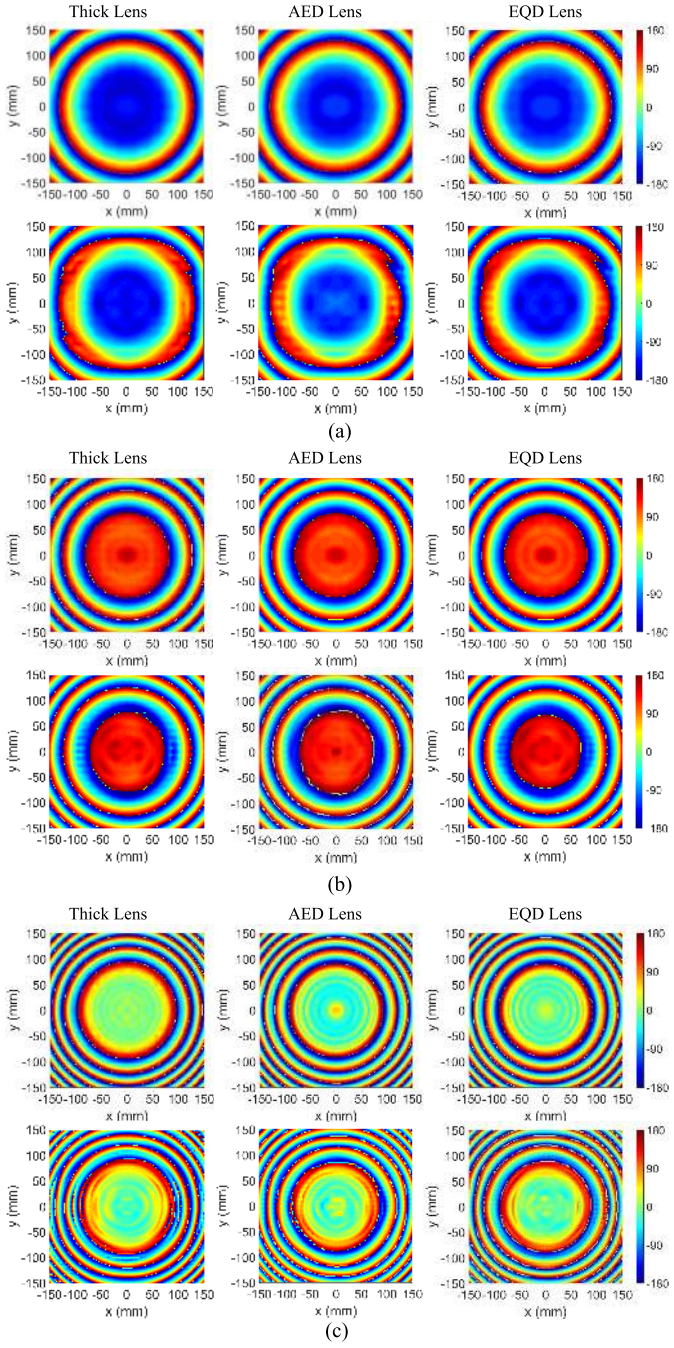

Fig. 13. Measured near-field phase distribution at 15, 22, and 33 GHz, respectively, compared with the simulated results. (a) Simulation (top) and measurement (bottom) at 15 GHz. (b) Simulation (top) and measurement (bottom) at 22 GHz. (c) Simulation (top) and measurement (bottom) at 33 GHz.

frequency range. The increased loss is partly attributable to the increased insertion loss of the AED when the patch size approached the periodicity [see Fig. 5(c)]. This could be overcome by using a high-permittivity PCB to allow smaller patches. The second reason for the increased loss is the increased mismatch between the free space and the dielectric media, caused by the increased permittivity of the inner rings of the AED lens. An impedance matching layer can be added to improve the gain [32]; furthermore, the matching layer can also be additively manufactured.

Fig. 13 shows the holographic phase profile displaying the phase distribution in the plane that is normal to the boresight direction at 15, 22, and 33 GHz. Good agreement is observed between the simulation and measured results, which confirms that uniform phase distribution is achieved in the effective apertures of all three lenses. This indicates that the three lenses function equally well when transforming the quasi-spherical waves (radiated by their feeds) into plane waves. It is worthwhile to note that the phase profile at 33 GHz [see Fig. 13(c)] shows a slight nonuniform phase distribution in the regions of the outer rings of the lenses. This indicates that the fabricated outermost rings did not have the desired effective permittivity profiles needed to satisfy the uniform phase condition. However, due to the varied periodicity unit cell, the inner rings still function as the homogeneous dielectrics with the desired effective permittivities, which maintains the uniform phase distribution. Also, small phase discrepancies begin to appear at each ring center, where the ring width becomes relatively large compared with the wavelength and begins to degrade the lens' performance. However, this nonuniform phase region remains small, and therefore, all the lenses still provide good gain improvement at the higher end of the frequency range. The performance of the fabricated lenses at high frequencies could be further improved if the same volume fraction of ABS is achieved with smaller unit cells, so the outer rings would maintain their effective medium values that they have at lower frequencies, and the small unit cell also permits us to use thinner rings for smoother variation of the permittivity profile. High-resolution AM facilities, which can fabricate objects with fine features, can be used to fabricate the reduced the size of individual air voids or meshes in relatively small values and, therefore, produce GRIN lenses with a wider bandwidth.

VI. Conclusion and Discussion

This article has presented the design and fabrication of flat GRIN lenses with an ultrawideband behavior that spans over a 108% fractional bandwidth. The design equation has been derived via the frequency-independent GRIN ray optics theory. The GRIN lenses were additively manufactured, and the partially infilled printing realizes the dielectric rings with tailored permittivities to form the flat GRIN medium. The varied periodicity unit cell realizes a gradually increased unit cell size from the center to the outer region of the lens, so the inner region still functions at high frequencies even when the outer region does not provide the desired effective permittivity value. The dielectric property of the partially infilled geometries has been investigated and proven via dielectric property measurements. Besides using partially infilled structures, ε_{reff} can be further tailored by using the AED approach. The AEDs have been conveniently realized by combining 3-D-printed structures with commercially available PCB laminate materials. The equivalence between AED materials and their EQDs has been verified by the agreement in the transmission performance, which enables us to implement the AEDs in the flat GRIN lens application.

Measurement results have shown the advantages of the ultrawideband GRIN lens in beam collimating, and all three

lenses had realized gain from 15.1 to 23.6 dBi between 12 and 40 GHz, fed by OEWGs, which increased the gain of the OEWG feeds by 8.7 up to 15.6 dB. Furthermore, all lenses offered high antenna efficiency of 82% averaged between 12 and 40 GHz. Additional time-domain measurement and the fidelity factor that quantifies the signal distortion introduced by the lens can be examined, if desired, to show the wideband true-time-delay operation [33]–[35]; however, fully fledged investigation of the time-domain performance of the lens is beyond the scope of this work. The equivalent performance characteristics of the three lenses clearly demonstrate the benefits of utilizing high-permittivity materials to reduce their thicknesses by ∼30% and their mass by ∼20%. Furthermore, the results also prove the concept of using the AED approach to replace the dielectric materials in an ultrawideband frequency range when the required permittivity values are not commercially available. The AED approach is scalable and can be easily combined with materials with different permittivity ranges. For instance, the AED approach can be applied to the PREMIX ($\varepsilon_r = 4.4$) materials to create new AED materials that have $\varepsilon_{reff} > 4.4$. The number of metallic layers can also be increased to realize the required permittivity values. The AED approach is also compatible with the multilayer PCB or low-pass frequency selective surfaces (FSS)-based approaches [34], [36] for the applications that require thin lenses or a small f/D value to realize compact lens antenna systems. This gives us extra degrees of freedom to select dielectric materials, which is certain to benefit the task of RF component design.

The lenses in this work had $f/D = 1.25$. Generally, a smaller f/D lens would require a thinner ring width to realize a smoother permittivity profile to ensure the wideband and high gain performance. This is because the permittivity variation in a lens with a small f/D is greater than the variation in a lens with a large f/D value. A lens with decreased f/D or thickness leads to an increased permittivity variation range, which also increases the reflection due to the impedance mismatch between the free space and the high-index medium. This could be the potential limitation of the AED approach since a high-index medium requires large metallic patches, but it also introduces additional loss due to the mismatch. A low-profile wideband impedance matching layer that does not significantly increase the lens thickness is highly desirable.

The proposed AM approach is a low-cost technique, which is well-suited for fast automated repeatable design and manufacturing. It has the potential to significantly transform the manufacturing processes and to significantly shorten the time that it takes for innovative new technologies to reach consumers while reducing labor costs and waste.

APPENDIX

We assume that the angle between the path where the ray enters the lens and the focal axis is θ (see Fig. 1). At P_1, according to Snell's law, it follows that

$$\sin\theta \cdot 1 = \sin\varphi_1 \cdot n_1 \tag{5}$$

where n_1 is the reflective index at P_1. φ_1 is the angle between the tangent to the ray and the y-axis.

If the ray path in the GRIN medium has a function $y = f(x)$, the length of the ray path from P_1 to P_2 can be expressed as

$$\int_{P_1}^{P_2} nds = \int_{x_1}^{x_2} n\sqrt{1+\left(\frac{df}{dx}\right)^2}\,dx = \mathcal{F}(x)dx. \tag{6}$$

The lens can be considered as a quarter-pitch GRIN fiber, and therefore, the ray from P_1 to P_2 has the shortest optical path, and the path length satisfies the Euler–Lagrange equation:

$$\frac{\partial\mathcal{F}}{\partial x} = \frac{d}{dx}\left(n\sqrt{1+\left(\frac{df}{dx}\right)^2}\right) = \frac{n\cdot\frac{df}{dx}}{\sqrt{\left(\frac{df}{dx}\right)^2+1}} = c \tag{7}$$

where c is a constant. For $f(x)$ at P_1, (df/dx) is the slope of $f(x)$ with respect to x. Thus, (7) can be rewritten as

$$\frac{\partial\mathcal{F}}{\partial \mathrm{x}} = \frac{n_1\cdot\cot\varphi_1}{\sqrt{\cot^2\varphi_1+1}} = n_1\cdot\cos\varphi_1 = c. \tag{8}$$

Similarly, we have $n_2\cdot\cos\varphi_2 = c$ at P_2, where φ_2 is the angle between the ray path outside the lens and the normal vector of the lens plane. Since the ray path outside the lens is also normal to the lens plane, $\varphi_2 = 0$, and we have $n_2 = c$. Substituting this into (8) results in the relation $n_1\cdot\cos\varphi_1 = n_2$, and combining with (5), we have

$$n_2^2 = n_1^2 - \sin^2\theta = \varepsilon_{r1} - \sin^2\theta \tag{9}$$

where ε_{r1} is the permittivity at P_1.

Meanwhile, substituting $n_2 = c$ into (7), (df/dx) can be expressed as

$$\frac{df}{dx} = \frac{n_2}{\sqrt{n^2-n_2^2}}. \tag{10}$$

Therefore, (6) can be rewritten as

$$\int_{P_1}^{P_2} nds = \int_{x_1}^{x_2}\frac{n^2}{\sqrt{n^2-n_2^2}}dx = \int_{x_1}^{x_2}\frac{n^2}{\sqrt{n^2-(\varepsilon_{r1}-\sin^2\theta)}}dx. \tag{11}$$

Since P_1 and P_2 are the two points on the ray path $y = f(x)$, they satisfy

$$\begin{aligned} T = f(x_2) - f(x_1) &= \int_{x_1}^{x_2}\frac{df}{dx}dx = \int_{x_1}^{x_2}\frac{n_2}{\sqrt{n^2-n_2^2}}dx \\ &= \int_{x_1}^{x_2}\frac{\sqrt{\varepsilon_{r1}-\sin^2\theta}}{\sqrt{n^2-(\varepsilon_{r1}-\sin^2\theta)}}dx. \end{aligned} \tag{12}$$

In order to solve (12), it requires determining the relationship between x_1, x_2, and n. We assume that the relative permittivity varies linearly in the short region from x_1 to x_2, and it satisfies

$$a = \frac{\varepsilon_{r1}-\varepsilon_{r2}}{x_2-x_1} = \frac{\sin^2\theta}{x_2-x_1} \tag{13}$$

$$x_2 = \frac{\sin^2\theta + ax_1}{a} \tag{14}$$

where a is a constant. For a random point x between x_1 and x_2, the relative permittivity at x also satisfies

$$-a = \frac{\varepsilon_r - \varepsilon_{r1}}{x - x_1} \tag{15}$$

$$\varepsilon_r = \varepsilon_{r1} - a(x - x_1). \tag{16}$$

Since $n^2 = \varepsilon_r$, we first substitute (14) and (16) into (11) and then carry out the integration

$$\int_{P_1}^{P_2} nds = \int_{x_1}^{x_2} \frac{\varepsilon_{r1} - a(x - x_1)}{\sqrt{\varepsilon_{r1} - a(x - x_1) - \left(\varepsilon_{r1} - \sin^2\theta\right)}} dx = \frac{\sin\theta\left(6\varepsilon_{r1} - 4\sin^2\theta\right)}{3a}. \tag{17}$$

Similarly, substituting (14) and (16) into (12) and carrying out the integration, we get

$$a = \frac{2\sin\theta\sqrt{\varepsilon_{r1} - \sin^2\theta}}{T}. \tag{18}$$

Next, we substitute (18) into (17), and we can obtain the expression of the path length inside the GRIN medium as follows:

$$\int_{P_1}^{P_2} nds = \frac{T\left(3\varepsilon_{r1} - 2\sin^2\theta\right)}{3\sqrt{\varepsilon_{r1} - \sin^2\theta}}. \tag{19}$$

ACKNOWLEDGMENT

The authors thank PREMIX for providing the PREPERM TP20280 3D-printing filament.

REFERENCES

[1] D. T. Moore, "Gradient-index optics: A review," *Appl. Opt.*, vol. 19, no. 7, p. 1035, Apr. 1980.

[2] F.-Y. Meng *et al.*, "Automatic design of broadband gradient index metamaterial lens for gain enhancement of circularly polarized antennas," *Prog. Electromagn. Res.*, vol. 141, pp. 17–32, Jul. 2013.

[3] S. Jain, M. Abdel-Mageed, and R. Mittra, "Flat-lens design using field transformation and its comparison with those based on transformation optics and ray optics," *IEEE Antennas Wireless Propag. Lett.*, vol. 12, pp. 777–780, 2013.

[4] M. K. T. Al-Nuaimi, W. Hong, and Y. Zhang, "Design of high-directivity compact-size conical horn lens antenna," *IEEE Antennas Wireless Propag. Lett.*, vol. 13, pp. 467–470, 2014.

[5] C. Mateo-Segura, A. Dyke, H. Dyke, S. Haq, and Y. Hao, "Flat Luneburg lens via transformation optics for directive antenna applications," *IEEE Trans. Antennas Propag.*, vol. 62, no. 4, pp. 1945–1953, Apr. 2014.

[6] H. F. Ma, X. Chen, H. S. Xu, X. M. Yang, W. X. Jiang, and T. J. Cui, "Experiments on high-performance beam-scanning antennas made of gradient-index metamaterials," *Appl. Phys. Lett.*, vol. 95, no. 9, pp. 1–4, 2009.

[7] M. Jiang, Z. N. Chen, Y. Zhang, W. Hong, and X. Xuan, "Metamaterial-based thin planar lens antenna for spatial beamforming and multi-beam massive MIMO," *IEEE Trans. Antennas Propag.*, vol. 65, no. 2, pp. 464–472, Feb. 2017.

[8] H. D. Hristov and M. H. A. J. Herben, "Millimeter-wave fresnel-zone plate lens and antenna," *IEEE Trans. Microw. Theory Techn.*, vol. 43, no. 12, pp. 2779–2785, Dec. 1995.

[9] J. Xu, Z. N. Chen, and X. Qing, "270-GHz LTCC-integrated high gain cavity-backed fresnel zone plate lens antenna," *IEEE Trans. Antennas Propag.*, vol. 61, no. 4, pp. 1679–1687, Apr. 2013.

[10] C. G. M. Ryan, M. R. Chaharmir, J. Shaker, J. R. Bray, Y. M. M. Antar, and A. Ittipiboon, "A wideband transmitarray using dual-resonant double square rings," *IEEE Trans. Antennas Propag.*, vol. 58, no. 5, pp. 1486–1493, May 2010.

[11] A. H. Abdelrahman, A. Z. Elsherbeni, and F. Yang, "High-gain and broadband transmitarray antenna using triple-layer spiral dipole elements," *IEEE Antennas Wireless Propag. Lett.*, vol. 13, pp. 1288–1291, 2014.

[12] J. H. Kim, C.-H. Ahn, and J.-K. Bang, "Antenna gain enhancement using a holey superstrate," *IEEE Trans. Antennas Propag.*, vol. 64, no. 3, pp. 1164–1167, Mar. 2016.

[13] T. Hayat, M. U. Afzal, A. Lalbakhsh, and K. P. Esselle, "3-D-printed phase-rectifying transparent superstrate for resonant-cavity antenna," *IEEE Antennas Wireless Propag. Lett.*, vol. 18, no. 7, pp. 1400–1404, Jul. 2019.

[14] H. F. Ma and T. J. Cui, "Three-dimensional broadband and broad-angle transformation-optics lens," *Nature Commun.*, vol. 1, no. 1, p. 124, Dec. 2010.

[15] O. Quevedo-Teruel *et al.*, "Transformation optics for antennas: Why limit the bandwidth with metamaterials?" *Sci. Rep.*, vol. 3, no. 1, Dec. 2013, Art. no. 1903.

[16] K. S. Kelleher and C. Goatley, "Dielectric lens for microwaves," *Electronics*, pp. 142–145, Aug. 1955.

[17] D. R. Smith, J. J. Mock, A. F. Starr, and D. Schurig, "Gradient index metamaterials," *Phys. Rev. E, Stat. Phys. Plasmas Fluids Relat. Interdiscip. Top.*, vol. 71, no. 3, Mar. 2005, Art. no. 036609.

[18] T. Driscoll *et al.*, "Free-space microwave focusing by a negative-index gradient lens," *Appl. Phys. Lett.*, vol. 88, no. 8, Feb. 2006, Art. no. 081101.

[19] H. F. Ma, B. G. Cai, T. X. Zhang, Y. Yang, W. X. Jiang, and T. J. Cui, "Three-dimensional gradient-index materials and their applications in microwave lens antennas," *IEEE Trans. Antennas Propag.*, vol. 61, no. 5, pp. 2561–2569, May 2013.

[20] Y. Su and Z. N. Chen, "A flat dual-polarized transformation-optics beamscanning Luneburg lens antenna using PCB-stacked gradient index metamaterials," *IEEE Trans. Antennas Propag.*, vol. 66, no. 10, pp. 5088–5097, Oct. 2018.

[21] Q.-W. Lin and H. Wong, "A low-profile and wideband lens antenna based on high-refractive-index metasurface," *IEEE Trans. Antennas Propag.*, vol. 66, no. 11, pp. 5764–5772, Nov. 2018.

[22] D. Isakov, C. J. Stevens, F. Castles, and P. S. Grant, "3D-printed high dielectric contrast gradient index flat lens for a directive antenna with reduced dimensions," *Adv. Mater. Technol.*, vol. 1, no. 6, Sep. 2016, Art. no. 1600072.

[23] M. Liang, W.-R. Ng, K. Chang, K. Gbele, M. E. Gehm, and H. Xin, "A 3-D Luneburg lens antenna fabricated by polymer jetting rapid prototyping," *IEEE Trans. Antennas Propag.*, vol. 62, no. 4, pp. 1799–1807, Apr. 2014.

[24] G. Du, M. Liang, R. A. Sabory-Garcia, C. Liu, and H. Xin, "3-D printing implementation of an X-band eaton lens for beam deflection," *IEEE Antennas Wireless Propag. Lett.*, vol. 15, pp. 1487–1490, 2016.

[25] X. Chen, H. F. Ma, X. Y. Zou, W. X. Jiang, and T. J. Cui, "Three-dimensional broadband and high-directivity lens antenna made of metamaterials," *J. Appl. Phys.*, vol. 110, no. 4, Aug. 2011, Art. no. 044904.

[26] S. Zhang, R. K. Arya, S. Pandey, Y. Vardaxoglou, W. Whittow, and R. Mittra, "3D-printed planar graded index lenses," *IET Microw., Antennas Propag.*, vol. 10, no. 13, pp. 1411–1419, Oct. 2016.

[27] W. B. Weir, "Automatic measurement of complex dielectric constant and permeability at microwave frequencies," *Proc. IEEE*, vol. 62, no. 1, pp. 33–36, Jan. 1974.

[28] S. Zhang, W. Whittow, and J. C. Vardaxoglou, "Additively manufactured artificial materials with metallic meta-atoms," *IET Microw., Antennas Propag.*, vol. 11, no. 14, pp. 1955–1961, Nov. 2017.

[29] C. A. Fernandes, E. B. Lima, and J. R. Costa, "Broadband integrated lens for illuminating reflector antenna with constant aperture efficiency," *IEEE Trans. Antennas Propag.*, vol. 58, no. 12, pp. 3805–3813, Dec. 2010.

[30] S. Zhang, D. Cadman, and J. Y. C. Vardaxoglou, "Additively manufactured profiled conical horn antenna with dielectric loading," *IEEE Antennas Wireless Propag. Lett.*, vol. 17, no. 11, pp. 2128–2132, Nov. 2018.

[31] P. V. Prasannakumar, M. A. Elmansouri, and D. S. Filipovic, "Broadband reflector antenna with high isolation feed for full-duplex applications," *IEEE Trans. Antennas Propag.*, vol. 66, no. 5, pp. 2281–2290, May 2018.

[32] Y. He and G. V. Eleftheriades, "Matched, low-loss, and wideband graded-index flat lenses for millimeter-wave applications," *IEEE Trans. Antennas Propag.*, vol. 66, no. 3, pp. 1114–1123, Mar. 2018.

[33] M. Li and N. Behdad, "Wideband true-time-delay microwave lenses based on metallo-dielectric and all-dielectric lowpass frequency selective surfaces," *IEEE Trans. Antennas Propag.*, vol. 61, no. 8, pp. 4109–4119, Aug. 2013.
[34] M. Li, M. A. Al-Joumayly, and N. Behdad, "Broadband true-time-delay microwave lenses based on miniaturized element frequency selective surfaces," *IEEE Trans. Antennas Propag.*, vol. 61, no. 3, pp. 1166–1179, Mar. 2013.
[35] G. Quintero, J.-F. Zurcher, and A. K. Skrivervik, "System fidelity factor: A new method for comparing UWB antennas," *IEEE Trans. Antennas Propag.*, vol. 59, no. 7, pp. 2502–2512, Jul. 2011.
[36] M. A. Al-Joumayly and N. Behdad, "Wideband planar microwave lenses using sub-wavelength spatial phase shifters," *IEEE Trans. Antennas Propag.*, vol. 59, no. 12, pp. 4542–4552, Dec. 2011.

Shiyu Zhang received the Ph.D. degree from Loughborough University, Loughborough, U.K., in 2014.

Following graduation, he worked as a Research Associate with Loughborough University, where he is currently with the Wolfson School of Mechanical, Electrical, and Manufacturing Engineering. His current research interests include engineered electromagnetic structures (metamaterials, metasurfaces, and frequency selective surfaces), antennas and RF circuit components, additive manufacturing (3-D-printing), and wearable antennas and electronic systems.

He received the EPSRC Doctoral Prize Research Fellowship 2015, and he was the recipient of the first runner up of the 2013 Loughborough Antennas and Propagation Conference (LAPC) IET Best Student Paper award. He served as the Technical Program Committee member for the LAPC in 2017 and 2018.

Ravi Kumar Arya (Member, IEEE) received the B.E. degree from Delhi Technological University, Delhi, India, in 2003, the M.Tech. degree in RF and microwave engineering from the Indian Institute of Technology, Kharagpur, India, in 2006, and the Ph.D. degree in electrical engineering from the Pennsylvania State University, State College, PA, USA, in 2017.

After completing his B.E. degree, he worked with Electronics Corporation of India Limited, New Delhi, India, for six months and then with Center for Development of Telematics (C-DOT), Bengaluru, India, from 2006 to 2010. In 2017, he worked with Isotropic Systems, Linthicum, MD, USA, as an RF Optical Design Engineer, where he developed various antennas for satellite communication systems, wrote various analysis tools for lens and array design, implemented and managed Amazon Web Services (AWS) computer resources for the company. In 2019, he joined the National Institute of Technology (NIT) Delhi, New Delhi, India, where he is currently an Assistant Professor with the Department of Electronics and Communication Engineering. He has published several technical papers in highly ranked journals and refereed conference proceedings, including three book chapters. His research interests include RF circuit design, antenna design, lens design, and the analysis of frequency-selective surfaces.

William G. Whittow (Senior Member, IEEE) received the B.Sc. degree in physics and the Ph.D. degree in computational electromagnetics from the University of Sheffield, Sheffield, U.K., in 2000 and 2004, respectively.

From 2004 to 2012, he was a Research Associate with Loughborough University, Loughborough, U.K. In 2012, he became a Lecturer with Electronic Materials Integration, University of Loughborough. He became a Senior Lecturer in 2014, a Reader (Associate Professor) in 2018, and a Professor in radiofrequency materials with the Wolfson School of Mechanical, Electrical and Manufacturing Engineering, Loughborough University. He is a named Investigator on EPSRC grants totaling in excess of £9m. He has authored approximately 250 peer-reviewed journal and conference papers in topics related to electromagnetic materials, synthetic dielectrics, dielectric measurements, 3-D-printing, wearable antennas, VHF antennas, specific absorption rate, finite difference time domain (FDTD), specific absorption rate, metamaterials, heterogeneous substrates, embroidered antennas, inkjet printing, electromagnetic compatibility, RFID tags, phantoms, and genetic algorithms.

Dr. Whittow was the Coordinating Chair of the Loughborough Antennas and Propagation Conference (LAPC) from 2007 to 2011. He has served as an Associate Editor for *IET's Electronics Letters* and also *Microwaves, Antennas and Propagation*. He serves on the technical program committees for several IEEE international conferences. He has been asked to give more than 20 invited conference presentations; a four days invited workshop on bioelectromagnetics and teaches about dielectric measurements at the European School of Antennas. In 2017, he won the Women in Engineering Men As Allies Award and he is the inaugural male Associate Fellow of Women's Engineering Society (WES). He is a Senior Fellow of the Higher Education Academy. Approximately 80 of his academic journal papers can be freely downloaded here: http://publications.lboro.ac.uk/publications/all/collated/elwgw.html

Darren Cadman received the Ph.D. degree from the Institute of Microwaves and Photonics, University of Leeds, U.K., in 2003, investigating the optical control of microstrip electromagnetic bandgap structures.

In 2007, he worked at Filtronic Compound Semiconductors Ltd., Newton Aycliffe, County Durham, U.K., after which he took up the post of managing the Innovative Electronics Manufacturing Research Center based at Loughborough University, Loughborough, U.K. In 2016, he took up the post of Program Manager for the U.K.'s EPSRC funded project "Synthesizing 3D Metamaterials for RF, Microwave, and THz Applications" led by Loughborough University. His current research interest includes the application of additive manufacturing processes and materials to create microwave passive componentry, with a focus on ceramics.

Raj Mittra (Life Fellow, IEEE) is a Professor with the Electrical and Computer Engineering Department, University of Central Florida (UCF), Orlando, FL, USA, where he is the Director of the Electromagnetic Communication Laboratory. He also holds an appointment at the Pennsylvania State University, University Park, PA, USA. Prior to joining Penn State, he was a Professor with the Electrical and Computer Engineering, University of Illinois in Urbana Champaign, Urbana/Champaign, IL, USA, from 1957 through 1996. He is a Principal Scientist and President of RM Associates, Orlando, FL, USA, a consulting company founded in 1980, which provides services to industrial and governmental organizations, both in the U.S. and abroad.

He is a Past-President of antennas and propagation (AP)-S, and he has served as the Editor for the Transactions of the Antennas and Propagation Society. He is currently the Editor-in-Chief of *FERMAT*, an e-journal published by the UCF with the endorsement of the IEEE/AP Education Society. He has received numerous awards and medals from the IEEE, as well as from the AP Society. He was recently recognized for his contributions by the URSI with the Rawer medal, and the Alexander Graham Bell award from the IEEE Foundation. A partial list of his recent publications may be found via Google Scholar Search.

J. (Yiannis) C. Vardaxoglou (Fellow, IEEE) received the B.Sc. degree in mathematical physics in 1982 and the Ph.D. degree in electronics in 1985 from the University of Kent, Kent, U.K.

He joined Loughborough University, Loughborough, U.K., as a Lecturer in 1988, was promoted to Senior Lecturer in 1992, and to a Professor of Wireless Communications, a post he holds since 1998. He served as the Dean for the School of Electronic, Electrical and Systems Engineering, Loughborough University from 2006 to 2012. He established the 32-year-old Wireless Communications Research (WiCR) group at Loughborough University and founded the Centre for Mobile Communications Research (CMCR). He has served as a Consultant for various industries, holds six patents, and is the Founder/Technical Director of Antrum Ltd. His current research focuses primarily on metamaterial structures and additive manufacturing (3-D printing) for RF/micro-/mm-wave engineering. He has published over 400 refereed journals and conference proceeding papers (with over 8775 citations) and has written a seminal book on frequency selective surfaces (FSS).

Dr. Vardaxoglou was awarded a prestigious EPSRC's Grand Challenge £5M (FEC) award "Synthesizing 3D Metamaterials for RF, Microwave, and THz Applications" (http://gow.epsrc.ac.uk/NGBOViewGrant.aspx?GrantRef=EP/N010493/1). He is the Director of SYMETA research center (www.symeta.co.uk) funded by an EPSRC Grand Challenge award, researching wide-ranging topics applicable to cutting-edge wireless communications technology. SYMETA collaborates with many internationally leading companies and universities. He has attracted research funding from the industry and has been awarded 20 EPSRC research grants. He was the Chairman of the Executive Committee of the IET's Antennas and Propagation Professional Network in the U.K. and chaired the IEEE's distinguished lecturer program of the Antennas and Propagation Society (APS) for five years. He founded the Loughborough Antennas & Propagation Conference (LAPC), which has been running since 2005. He has chaired numerous IEE//IET events and has served on the Steering Committee of the European Conference on Antennas and Propagation (EuCAP). He was the General Chair of EuCAP '07. He is a Fellow of the Royal Academy of Engineers (FREng) and a Fellow of the Institute of Electrical and Electronics Engineers (FIEEE).